IEEE Access
Multidisciplinary ⋮ Rapid Review ⋮ Open Access Journal

Received August 24, 2020, accepted September 5, 2020, date of publication September 14, 2020, date of current version November 6, 2020.

Digital Object Identifier 10.1109/ACCESS.2020.3023763

Wide-Speed Range Operation of PM Vernier Machines Using Wye and Wye-Delta Winding Configurations

ARSALAN ARIF[1], NOMAN BALOCH[1], MUHAMMAD AYUB[1,2], AND BYUNG-IL KWON[1], (Senior Member, IEEE)

[1]Department of Electrical and Electronic Engineering, Hanyang University, Ansan 15588, South Korea
[2]Department of Electronic Engineering, Balochistan University of Information Technology, Engineering and Management Sciences (BUITEMS), Quetta 87300, Pakistan

Corresponding author: Byung-Il Kwon (bikwon@hanyang.ac.kr)

This work was supported in part by the BK21PLUS Program through the National Research Foundation of Korea within the Ministry of Education, and in part by the National Research Foundation of Korea (NRF) Grant funded by the Korean Government (Ministry of Science) under Grant NRF-2020R1A2B5B01002400.

ABSTRACT This paper proposes two permanent magnet vernier machines (PMVM) operation modes, for wide-speed and high efficiency operation. In mode-1, the machine operates as a conventional PMVM with a wye connected stator winding mode. In mode-2, the machine stator winding is switched to a wye-delta winding mode. Contrary to the existing dual-inverter PMVM topology with two additional bidirectional thyristor switches, the proposed topology utilizes a single inverter with six additional bidirectional thyristor switches to change mode. A theoretical discussion of the proposed idea is further verified via finite element analysis (FEA) simulations. The basic electromagnetic characteristics, such as the flux linkage, back electromotive force, torque, and phase voltages of the machine are investigated using wye and wye-delta stator winding configurations, and subsequently, compared with the existing topology that used a dual-inverter PMVM. The FEA results show that the proposed PMVM has low over-all losses, consequently resulting in improved efficiency compared to the existing topology. The speed increases by almost 9 times using the proposed single-inverter PMVM. Transient analysis using FEA is also conducted in this paper.

INDEX TERMS High-efficiency, permanent magnet vernier machine, wide-speed range, wye-delta mode switching.

I. INTRODUCTION

Permanent magnet vernier machines (PMVMs) have earned significant research attention due to their special operating principle, referred to as the ''magnetic gearing effect'' [1]. Usually, PMVMs have higher number of rotor pole pairs compared to stator pole pairs and their operating frequencies are higher as compared to the general permanent magnet synchronous machines (PMSMs). A high operating frequency leads to a high reactance in the PMVMs, resulting in a low power factor. Therefore, an inverter with high rating is generally needed to drive the machine. PMVMs produce almost twice the back electromotive force (EMF) of conventional PMSMs, and thus, produce a higher torque density. This feature has made PMVMs a promising successor in direct-drive applications, such as electric vehicles (EVs) [2]. EVs are environmentally friendly and thus a considerable amount of research has been conducted to improve the equipment used in EVs [3]–[5].

Since the beginning, many novel topologies have been presented for increasing torque density in PMVMs [6]–[13]. PMVMs generally have low power factor issue. Numerous topologies have been proposed to address them. Dual-stator spoke-type vernier machines are presented for high-torque density and high power factors owing to their flux focusing effect [14]–[16].

A wide-speed range with constant power and high machine performance has always been the topic of interest for many researchers, considering EV applications. The wide-speed range operation of non-salient PM machines using winding switching was proposed in [17]; while winding switching for PMVMs was proposed in [18] to achieve a wide-speed range

The associate editor coordinating the review of this manuscript and approving it for publication was Ramani Kannan.

operation. In [18], before winding switching, the machine acted as a conventional three-phase PMVM. After winding switching, the inductance and back EMF of the machine decreased, and a wide-speed range operation was achieved. However, the efficiency of the machine was low during this operation. In [19], turn switching, and winding switching have been proposed for PMVMs to improve efficiency during wide-speed range operation for EV applications. This technique improved the low-efficiency problem associated with that of [18]; however, the tradeoff was increased cost due to the additional eight switches and dual-inverter topology.

Some researchers proposed changeover schemes: series-to parallel [20]–[23], wye-to-delta [24], [25], and tapped reconfiguration winding schemes [26]. A combined wye-delta connection was used in axial flux PM machines to increase their performance [27]; the output torque increased due to the increased winding factor and thus the efficiency ultimately increased. In [28], a hybrid wye-delta connection for a high voltage induction motor was described, to improve the efficiency of the machine. The performance of a conventional wye and combined wye-delta connected winding was analyzed and compared in a synchronous reluctance motor (SynRM) in [29]. In this literature, comparison was conducted for both normal and faulty conditions. The electromagnetic performance, compared to conventional three-phase wye winding configuration, was improved by combining the wye–delta stator winding configuration. Four prototype SynRMs were compared with identical iron lamination stacks in the stator and rotor [30]; the torque and efficiency were improved compared to the conventional machine.

This paper proposes two modes of operation for a PMVM: in mode-1, stator windings are connected in a wye configuration; in mode-2, the stator winding is switched to the wye-delta configuration for improved efficiency and wide-speed range operation. The machine achieves high torque in the low-speed region by configuring the machine stator winding as wye-connected and can obtain a wide-speed range by configuring the machine stator winding as wye-delta connected. A theoretical discussion and finite element analysis (FEA) were performed. The FEA results of the basic EMF, power, efficiency, and wide-speed range operation are compared with those of the existing dual-inverter PMVM topology.

II. MACHINE TOPOLOGY WITH WINDING CONFIGURATION AND WORKING PRINCIPLE

A. MACHINE TOPOLOGY

The outer rotor machine topology of the PMVM has been designed to show its wide speed-range characteristics, using wye to wye-delta switching, as shown in Fig. 1. The outer rotor topology can be directly coupled with the wheel of a small EV, which can result in a direct-drive machine for EV applications. The designed PMVM has a 24-slot stator, 46-pole outer PM rotor, and 2-pole stator armature winding. The winding configuration for the existing topology is shown

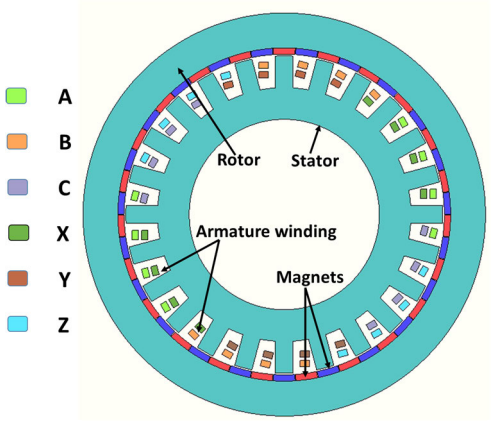

FIGURE 1. Machine topology of PMVM.

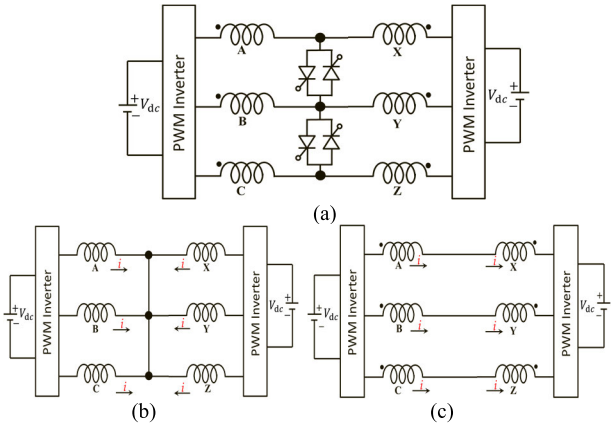

FIGURE 2. Winding configuration [18] (a) existing topology (b) cumulative mode (c) differential mode.

in Fig. 2(a) [18], while the cumulative and differential modes are shown in Fig. 2(b) and Fig. 2(c), respectively. The winding configuration of the proposed topology is shown in Fig. 3(a), and its two modes, specifically the wye and wye-delta mode, are shown in Fig. 3(b) and Fig. 3(c), respectively. The wye mode was used for low-speed operation, with high-torque, and the wye-delta mode used for high-speed operation, with low-torque. The main parameters of the machine are listed in Table 1.

B. WORKING PRINCIPLE

A PMVM has numerous rotor pole pairs, compared to the number of stator pole pairs, and its operation is based on the so-called ''magnetic gearing effect''. In PMVMs, a small movement of the rotor produces a fair amount of change in the flux, thus producing a higher back EMF as compared to a conventional PMSM. To produce the magnetic gearing effect, a PMVM must satisfy (1).

$$Z_r = Z_s - P \tag{1}$$

where P is the number of armature pole pairs, Z_r is the number of rotor pole pairs, and Z_s is the number of stator

TABLE 1. Main parameters of PMVM.

Item	Unit	Value
Rotor outer diameter	mm	254
Rotor inner diameter	mm	202
Stator outer diameter	mm	200
Stator inner diameter	mm	120
Stack length	mm	70
Rated speed	rpm	300
Rated torque	Nm	16.9
Rated Current	A	1.5
Rated Power	W	530.9
Rated Voltage	V	246.6
Rotor PM pole pairs	-	23
Stator slots	-	24
Turns/phase	-	280
Armature pole pairs	-	1
Airgap length	mm	1

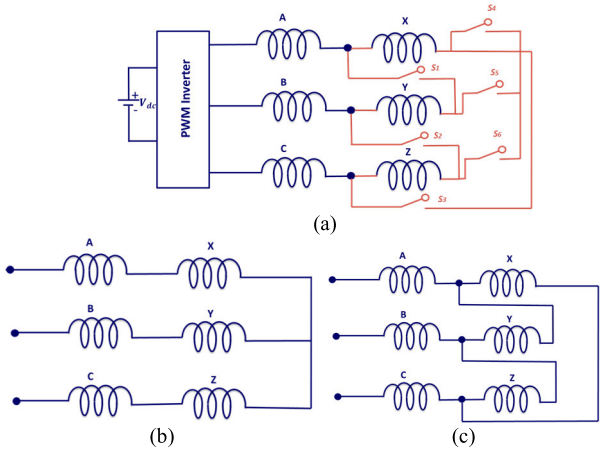

FIGURE 3. Winding configuration (a) proposed topology (b) wye mode (c) wye-delta mode.

slots. For this paper, P, Z_r, and Z_s, are chosen to be 1, 23 and, 24, respectively.

The air gap flux density of the proposed topology in the wye mode is shown in Fig. 4(a), whereas its harmonic spectra are shown in Fig. 4(b). It can be seen that the air gap has two major components: the 23rd pole pair component and modulated 1st pole pair component. These two components are the working harmonics and coupled with the corresponding harmonics of the stator MMF to produce a steady torque. Moreover, it should be noted, that both the existing and proposed topology used ferrite magnets to maintain a low machine cost.

In the proposed topology, the flux-weakening capability has been widely analyzed to extend the speed range, with supply voltage constraints. Generally, the stator winding of a three-phase machine has one of the winding connections, i.e., a wye or delta connection. Voltage utilization of the delta connection stator winding is $\sqrt{3}$ times that of the wye connection; full utilization of terminal voltage allows the speed range to be increased, compared to the wye connection stator winding.

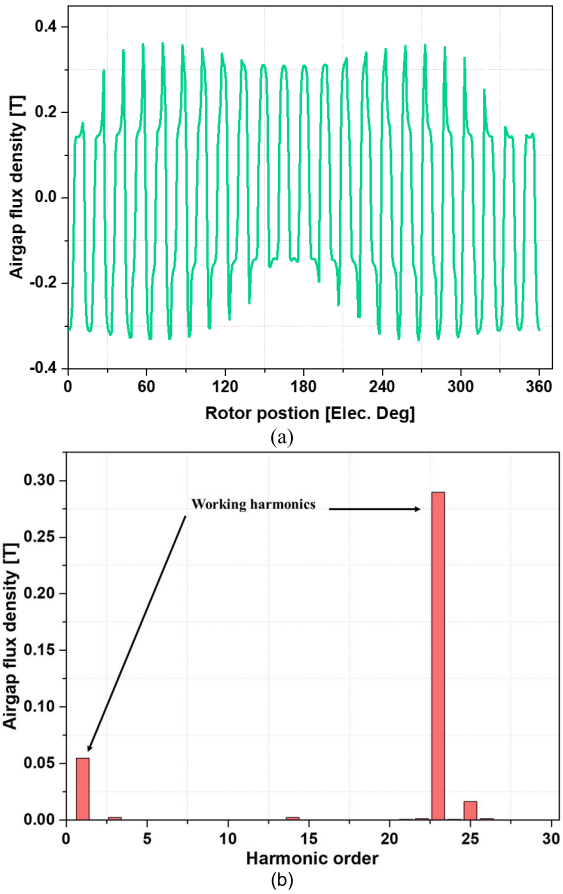

FIGURE 4. Airgap flux density (a) waveform (b) harmonic spectra.

During the entire wide-speed range, the d and q-axis currents are limited by the voltage and current limitations, that is, u_{lim} and i_{lim}, by neglecting the phase resistance, as defined below:

$$(\omega L_q i_q)^2 + (\omega L_d i_d + \omega \varphi_{pm})^2 \leq u_{lim}^2 \quad (2)$$

$$i_q^2 + i_d^2 \leq i_{lim}^2 \quad (3)$$

where L_d and L_q are the d and q-axis inductances, ω is the electrical angular velocity, φ_{pm} is the permanent magnet flux linkage, and i_d and i_q are the d and q-axis currents respectively.

Considering the two types of stator winding connections in the proposed topology. In wye mode stator winding, the maximum available phase voltage is $1/\sqrt{3}$ times that of line voltages, which limits the utilization factor of u_{lim}. Hence, the maximum constant power speed range is smaller. In wye-delta mode stator winding, the current in the delta-connected stator coils is $1/\sqrt{3}$ times of the wye-connected stator coils. Hence, the torque is lower, whereas, the utilization factor of i_{lim}, improves, consequently resulting in improved maximum constant power speed range. Similarly, since phase current in the delta winding coils is $1/\sqrt{3}$ times that of wye connected rated current, therefore the copper loss in the delta coils and iron loss in the delta coils region reduces. The speed and the

torque constant, and phase resistance, for the wye and delta connection coils can be summarized as follows:

resistance phase to phase (R):

$$\text{wye: delta} \rightarrow 4 : 4/3$$

speed constant (k_e):

$$\text{wye: delta} \rightarrow 2\sqrt{3} : 2$$

torque constant (k_m):

$$\text{wye: delta} \rightarrow 2\sqrt{3} : 2$$

The delta connected machine has a 1/3 times lower phase to phase resistance compared to the wye connected machine. Thus, copper losses are low and efficiency is high. The delta connected machine torque could be reduced by a factor of $\sqrt{3}$; with the same line current.

For three-phase delta connection stator windings, triple order EMF harmonics generate circulating current in the stator windings, and thus additional copper loss. The circulating current copper loss in the delta-connection stator coils is a drawback. The terminal voltage of the machine is limited by the inverter rating, and the delta connection winding utilizes more, compared to the wye connection. Hence, the back EMF of the delta-connected coils could be designed larger. In an electric machine, the electromagnetic power can be estimated as

$$P_{electomagnetic} = 3B_{EMF}.I_a \tag{4}$$

where B_{EMF} is the no-load back EMF and I_a is the phase current. In conventional medium to high-power machines, copper losses are much larger than iron losses; therefore, the phase current mainly affects the efficiency of the machine, which in the delta or wye-delta stator winding connection case is low because of the high back EMF. By decreasing the losses, the machine produces more torque for the same input power, and hence, the torque density increases. The wye to delta coils ratio could be further optimized for better performance. In the proposed topology, the PMVM operates in two modes, i.e., wye and wye-delta modes.

The phase voltages of the three-phase machine for A and X coil phases are given by (5) and (6), respectively [31].

$$\begin{aligned} V_{as} = {} & i_{as}r_s + L_{as}\frac{di_{as}}{dt} + \frac{1}{\sqrt{2}}(L_m + l_m)\frac{di_{xs}}{dt} \\ & - \frac{1+\sqrt{3}}{2\sqrt{2}}(L_m + l_m)\frac{di_{ys}}{dt} + \frac{-1+\sqrt{3}}{2\sqrt{2}}(L_m + l_m)\frac{di_{zs}}{dt} \\ & + \lambda_m\omega_e\cos(\omega_e t) \end{aligned} \tag{5}$$

$$\begin{aligned} V_{xs} = {} & i_{xs}r_s + L_{xs}\frac{di_{as}}{dt} + \frac{1}{\sqrt{2}}(L_m + l_m)\frac{di_{as}}{dt} \\ & + \frac{-1+\sqrt{3}}{2\sqrt{2}}(L_m + l_m)\frac{di_{bs}}{dt} - \frac{1+\sqrt{3}}{2\sqrt{2}}(L_m + l_m)\frac{di_{cs}}{dt} \\ & + \lambda_m\omega_e\cos\left(\omega_e t - {}^{\pi}/_{12}\right) \end{aligned} \tag{6}$$

The ABC and XYZ variables of the machine coils are transformed into stationary frame components q_1^s, d_1^s, q_2^s and d_2^s using (7) and (8), respectively.

$$\begin{bmatrix} V_{q1}^s \\ V_{d1}^s \\ V_{01}^s \end{bmatrix} = \frac{3}{2}\begin{bmatrix} 1 & -\frac{1}{2} & -\frac{1}{2} \\ 0 & -\frac{\sqrt{3}}{2} & \frac{\sqrt{3}}{2} \\ \frac{1}{2} & \frac{1}{2} & \frac{1}{2} \end{bmatrix}\begin{bmatrix} V_{as} \\ V_{bs} \\ V_{cs} \end{bmatrix} \tag{7}$$

$$\begin{bmatrix} V_{q2}^s \\ V_{d2}^s \\ V_{02}^s \end{bmatrix} = \frac{3}{2}\begin{bmatrix} \frac{1}{\sqrt{2}} & -\frac{1+\sqrt{3}}{2\sqrt{2}} & \frac{-1+\sqrt{3}}{2\sqrt{2}} \\ -\frac{1}{\sqrt{2}} & \frac{-1+\sqrt{3}}{2\sqrt{2}} & \frac{-1+\sqrt{3}}{2\sqrt{2}} \\ \frac{1}{2} & \frac{1}{2} & \frac{1}{2} \end{bmatrix}\begin{bmatrix} V_{xs} \\ V_{ys} \\ V_{zs} \end{bmatrix} \tag{8}$$

These stationary frame of reference equations can be transformed into a synchronous frame of reference using (9).

$$\begin{bmatrix} V_{q1}^e \\ V_{d1}^e \\ V_{q2}^e \\ V_{d2}^e \end{bmatrix} = \begin{bmatrix} \cos(\theta_e) & -\sin(\theta_e) & 0 & 0 \\ \sin(\theta_e) & \cos(\theta_e) & 0 & 0 \\ 0 & 0 & \cos(\theta_e) & -\sin(\theta_e) \\ 0 & 0 & \sin(\theta_e) & \cos(\theta_e) \end{bmatrix}\begin{bmatrix} V_{q1}^s \\ V_{d1}^s \\ V_{q2}^s \\ V_{d2}^s \end{bmatrix} \tag{9}$$

where V_{as} and V_{xs} are the voltages of coils A and X respectively, i_{as}, i_{bs} and i_{cs} are the currents in coils A, B, and C, respectively; i_{xs}, i_{ys} and i_{zs} are the currents in coils X, Y, and Z, respectively; L_{as} and L_{xs} are the self-inductances of coils A and X respectively; λ_m is the flux linkage due to permanent magnets; ω_e is the electrical angular velocity; L_m is the magnetizing inductance; r_s is the stator resistance; and I_m is the leakage inductance of the mutual component between the two three-phase windings.

The currents of coils ABC and XYZ in the wye mode are given as follows:

$$\begin{aligned} I_{aY} &= I_{xY} = I_m\sin\omega t \\ I_{bY} &= I_{yY} = I_m\sin(\omega t + 120) \\ I_{cY} &= I_{zY} = I_m\sin(\omega t + 240) \end{aligned} \tag{10}$$

where $I_{aY}, I_{bY}, I_{cY}, I_{xY}, I_{yY}$, and I_{zY} are the currents in coils ABC and XYZ, respectively, in the wye mode configuration.

The currents of winding ABC and XYZ in the wye-delta mode are given as follows:

$$\begin{aligned} I_{aY} &= I_m\sin\omega t \\ I_{bY} &= I_m\sin(\omega t + 120) \\ I_{cY} &= I_m\sin(\omega t + 240) \\ I_{x\Delta} &= \frac{I_m}{\sqrt{3}}\sin(\omega t - 30) \\ I_{y\Delta} &= \frac{I_m}{\sqrt{3}}\sin(\omega t + 90) \\ I_{z\Delta} &= \frac{I_m}{\sqrt{3}}\sin(\omega t + 210) \end{aligned} \tag{11}$$

where $I_{x\Delta}$, $I_{y\Delta}$, and $I_{z\Delta}$ are the currents in the delta XYZ coils.

From Fig. 3(a), the line-to-line EMF in the wye mode is given as:

$$\begin{aligned} E_{YY} &= E_a + E_x - E_b - E_y \\ &= 1 + 0.866 - j0.5 - j0.866 - 0 - j \\ &= 3.346Ee^{-j45} \end{aligned} \tag{12}$$

whereas the line-to-line EMF of the wye-delta mode, in Fig. 3(b), is given as:

$$\begin{aligned} E_{Y\Delta 1} &= E_a - E_x - E_b \\ &= 1 + 0.866 - j + 0.5 - j0.866 \\ &= 2.39Ee^{j51} \end{aligned} \tag{13}$$

The back EMF obtained in the wye mode divided by the back EMF obtained in the wye-delta mode gives the flux weakening ratio (F_w). From (12) and (13), this ratio is given as:

$$F_w = \frac{E_{wye(line\ to\ line)}}{E_{wye-delta}} \tag{14}$$

In the PMVM, the back EMF accounts for a large portion of phase voltages, limiting its operation for wide-speed range operation. The inverter limit is generally determined by the phase voltages of the machine obtained at the rated speed. The phase voltages should not increase beyond the available voltages of the inverter at any speed. Therefore, to use the PMVM for wide-speed range operation, the machine was switched from the wye mode to the wye-delta mode, which decreased the back EMF, and hence, decreased the phase voltages of the machine. Therefore, the speed of the machine in the proposed topology increased.

III. PERFORMANCE ANALYSIS OF PROPOSED PMVM AND COMPARISON WITH EXISTING TOPOLOGY

FEA was performed using the commercial software "Ansys Maxwell version 19" and "JMAG version 18.1". Initially, the FEA results pertaining to the wye and wye-delta modes of the machine were analyzed at a base speed of 300 rpm.

A. BACK EMF

A comparison of the back EMFs of the proposed topology and existing topology, at 300 rpm, is shown in Fig. 5. Fig. 5(a) shows the back EMF of the proposed topology in the wye and wye-delta modes, with rms values of 115 V and 87.9 V, respectively. Fig. 5(b) shows the back EMF of the existing topology in the cumulative and differential modes, with rms values of 115 V and 12.9 V, respectively.

While switching from the wye to wye-delta mode, the flux weakening ratio of the proposed topology was observed to be 1.31. However, the flux weakening ratio of the existing topology, while switching form the cumulative to differential mode, was 8.89. The flux weakening ratio of the proposed topology is less than that of the existing topology, owing to the lower drop in back EMF of the proposed topology after mode switching.

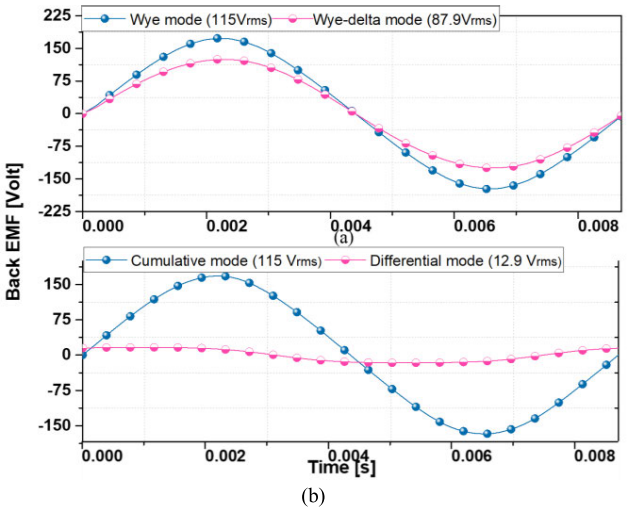

FIGURE 5. Comparison of Back EMFs (a) proposed topology (b) existing topology.

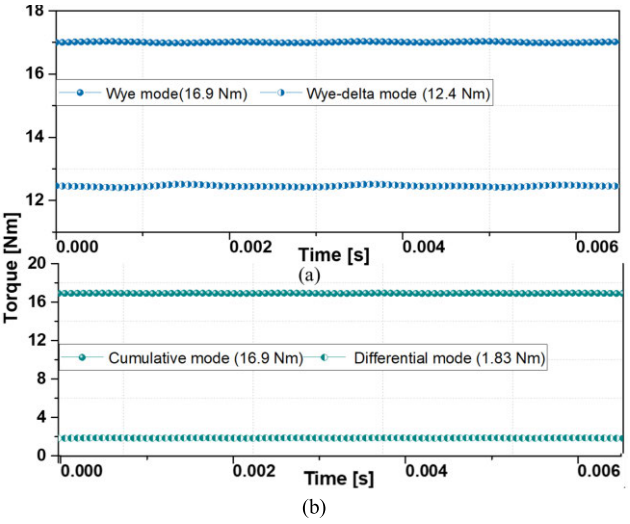

FIGURE 6. Comparison of Torques (a) proposed topology (b) existing topology.

B. TORQUE

A torque comparison of the proposed and existing topology is shown in Fig. 6. Furthermore, the torque of the proposed topology in the wye and wye-delta modes is shown in Fig. 6(a), and the torque of the existing topology is shown in Fig. 6(b). The torque ripple of the machine is low, as it is an inherent characteristic of PMVMs. Note that the power of the machine drops in the wye-delta mode.

Notably, after switching from the wye to wye-delta mode in the proposed topology, the torque is reduced from 16.9 Nm to 12.4 Nm. However, in the existing topology, the torque was reduced from 16.9 Nm to 1.83 Nm, while switching from the cumulative to differential mode. The torque dropped significantly after switching in the existing topology, compared to the proposed topology. Therefore, to maintain constant power, armature current of the machine was increased previously, which increased copper losses and hence, affected

the efficiency of the machine. In the proposed topology, torque is not significantly dropped, hence, armature current is not increased at any point beyond the rated current. Therefore, copper losses remain same and comparatively results in high-efficiency during wide-speed range operation. Therefore, the proposed topology results in better performance compared to the existing topology.

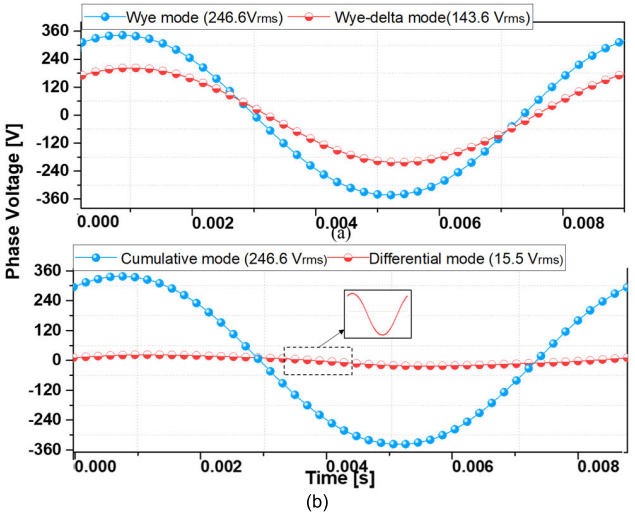

FIGURE 7. Comparison of phase voltages (a) proposed topology (b) existing topology.

C. PHASE VOLTAGES

A comparison of the phase voltages of the proposed and existing topology is shown in Fig. 7. The phase voltages of the machine in the wye and wye-delta modes of the proposed topology are shown in Fig. 7(a), while the phase voltages of the machine in the cumulative and differential modes of the existing topology are shown in Fig. 7(b). In the wye mode, the rms value of the phase voltage is 246.6 V; while in the wye-delta mode, the rms value of the phase voltage is 143.6V. The lower phase voltage provides an advantage for the wide-speed operation. This means that the inverter limit for the proposed topology is 246.6 V, which cannot be exceeded; otherwise, permanent damage to the inverter will occur. After switching from the wye to wye-delta mode the phase voltage is reduced to 143.6 V, ultimately creating the feasibility to increase the machine speed further, until the inverter limit of 246.6 V per phase is again reached. Once the inverter limit is reached, the machine speed cannot be increased further. The maximum speed achieved by the topology proposed in this paper was 2700 rpm.

Notably, the inverter limit for both topologies is the same, i.e., 246.6 V per phase. The cumulative mode in the existing topology is the same as the wye mode in the proposed topology; thus the electromagnetic characteristics of the wye mode in the proposed topology are the same as those of the cumulative mode in the existing topology.

However, the terminal voltage in the differential mode of the existing topology was 15.5 V, which is significantly low compared to the wye-delta mode of the proposed topology. Therefore, in comparison with the proposed topology, the existing topology has extra capacity to further increase the speed, until the inverter limit is reached. The maximum speed achieved by the existing topology was 5400 rpm, which is twice as high as that of the proposed topology.

D. FE-BASED TRANSIENT ANALYSIS DURING MODE SWITCHING

Analyzing the transient's effect at the instant of switching from one mode to another is important, as the proposed machine requires switching from the wye to wye-delta mode to achieve a wide-speed range and high efficiency. Therefore, transient simulations were performed to analyze the effect of switching on the inverter.

Switching was accomplished in three stages to avoid any huge spike occurring, furthermore, the controller waited for any of the three-phase currents to reach zero before the switch changed its state. Initially in stage 1, switches S1, S2 and S3 were maintained off, while S4, S5, and S6 were turned on, to put the circuit in wye mode as shown in Fig. 3(a). For mode change in stage 2, switch S1 was turned on, and switch S4 was turned off at current zero crossing, while the status of the remaining switches remained the same. In stage 3, switches S2 and S3 were turned on, and switches S5 and S6 were turned off, while the status of switches S1 and S4 remained the same to achieve the wye-delta mode configuration, as shown in Fig. 3(b). The switching sequences are listed in Table 2.

TABLE 2. Switching sequence for the mode change.

Switches	Stage 1	Stage 2	Stage 3
S1	OFF	ON	ON
S2	OFF	OFF	ON
S3	OFF	OFF	ON
S4	ON	OFF	OFF
S5	ON	ON	OFF
S6	ON	ON	OFF

Fig. 8 shows the proposed topology torque in the two modes. It can be observed that the torque is high in the wye mode and drops as soon as the machine is switched to the wye-delta mode. The simulation was performed for 4 electrical cycles. The machine runs in the wye mode for the first 2 cycles, but runs in the wye-delta mode for the last 2 cycles.

The phase voltage transients of the proposed machine during switching from the wye to wye-delta mode are shown in Fig. 9. Note that the machine can be switched between different modes under running conditions. Furthermore, a drop in the phase voltage in the wye-delta mode can be observed, which consequently allows the machine to operate in a wide-speed range. All simulation results shown in this paper have been performed using the current source. Therefore, the

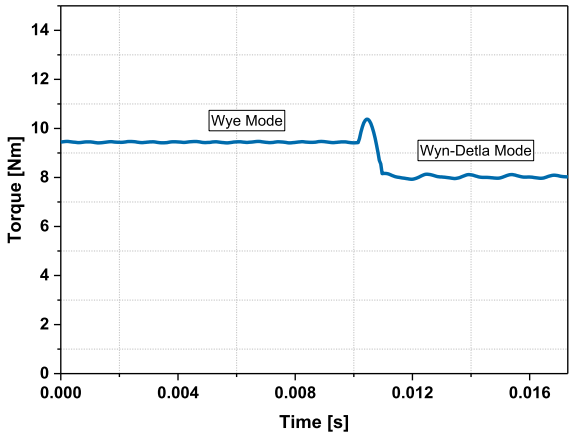

FIGURE 8. Proposed topology torque in two modes (Transient analysis).

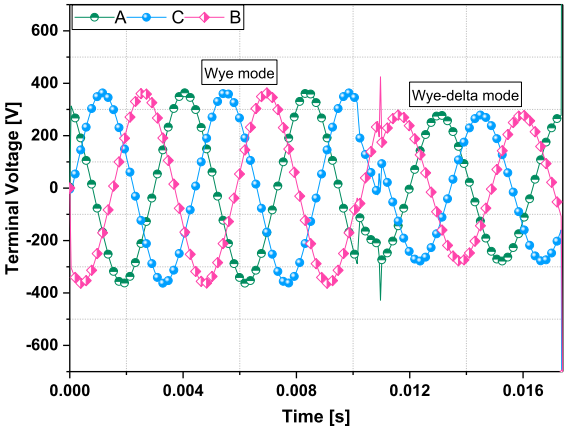

FIGURE 9. Phase voltages in two modes (Transient analysis).

transient effect during switching was visible in the phase voltages. At the switching instant, the peak phase voltages were observed to increase from 360 V to 425 V, approximately an 18% increase. Moreover, the transient period is very small (approximately a millisecond).

The transient analysis of the proposed machine shows that the machine can be smoothly switched from the wye to wye-delta mode, which will not damage or trip the inverter as switching transients only appear for a short instant.

IV. WIDE-SPEED RANGE ANALYSIS

Detailed FEA simulations were performed to explore the wide-speed characteristics of PMVMs using wye to wye-delta switching. Notably, although the maximum speed achieved by the existing topology was 5400 rpm, all the comparisons in this section were performed until 2700 rpm for the sake of clear observation between both topologies. A comparison of torque-speed curves for the proposed and existing topologies until 2700 rpm is shown in Fig. 10. It can be seen that both curves are almost the same.

A comparison of the total loss in the proposed and existing topologies is shown in Fig. 11. The losses tend to increase with the increasing speed of the machine. This is because the

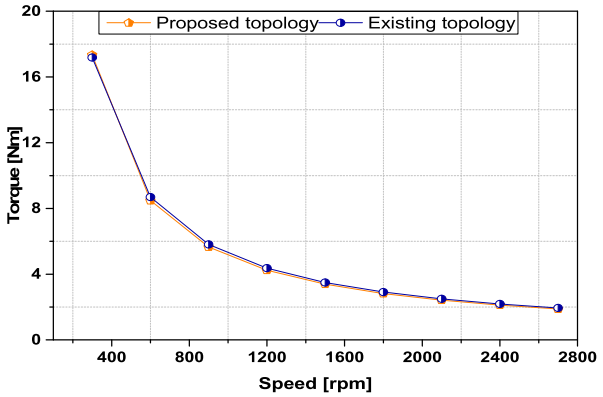

FIGURE 10. Comparison of torque-speed curves in proposed and existing topology.

TABLE 3. Overall comparison of proposed and existing topologies.

Parameter	Proposed Topology		Existing Topology	
Modes	Wye	Wye-delta	Cumulative	Differential
Back EMF (V)	115	87.9	115	12.9
Torque (Nm)	16.9	12.4	16.9	1.83
Phase voltages (V)	246.6	143.6	246.6	15.5
Efficiency (%)	94.4	88.4	94.4	61.7

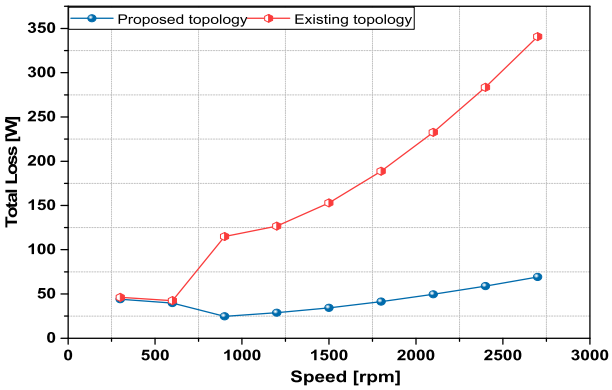

FIGURE 11. Comparison of total loss in proposed and existing topology.

core loss depends on the frequency, which increases as the machine speeds up. However, the copper losses are low and remain almost same throughout the wide-speed range. This is because the armature current was not increased beyond the rated point anywhere during the entire wide-speed range. It can be observed that the total losses in the existing topology are higher than those in the proposed topology, resulting in the proposed topology's higher efficiency. The core losses of the steel can be calculated using the Steinmetz equation (15) [32]

$$P_c = P_h + P_e = K_h f B^n + K_e f^2 B^2 \tag{15}$$

where $P_h P_e$, K_h, K_e, B, and f, are the hysteresis loss, eddy current loss, hysteresis loss coefficient, eddy current loss coefficient, flux density and frequency of the steel, respectively.

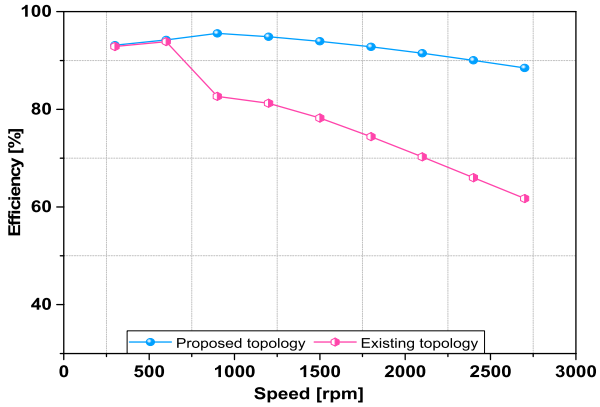

FIGURE 12. Comparison of efficiency curves in proposed and existing topology.

A comparison of the efficiency curves in the proposed and existing topologies is shown in Fig. 12. In this paper, efficiency (η) is calculated using (16).

$$\eta = \frac{P_{out}}{P_{out} + P_{cu} + P_{iron}} \times 100 \tag{16}$$

where P_{out}, P_{iron}, and P_{cu}, are the output power, iron losses, and copper losses, respectively. The copper losses were calculated by estimating the resistance of the winding per phase and armature currents, whereas the iron losses were calculated using FEA simulations.

Initially, it can be seen that the efficiency of both topologies is the same until switching occurs at 600 rpm in both cases; this can be explained as the cumulative mode in the existing topology is connected in wye mode configuration, which is the same as the proposed topology. Furthermore, the inverter limit for both topologies reached 600 rpm, i.e., switching in both topologies occurred at 600 rpm. For this reason, all curves in this section correspond, until 600 rpm.

It can be seen that the efficiency of the proposed topology is better than the existing topology; hence, the proposed topology offers a better performance than the existing topology. With increasing speed, the efficiency decreased gradually owing to an increase in the machine's core losses. The minimum efficiency of the proposed topology at the highest speed was 88.4%, while the minimum efficiency of the existing topology at 2700 rpm was 61.7%. Therefore, it is evident that the proposed topology provides better efficiency than the existing topology, over the entire wide-speed operation. The improved efficiency is explained by the core losses of the proposed topology being lower than those of the existing topology, over the entire wide speed range. The d-axis current was used in the proposed topology to reduce the toque in wye-delta mode to maintain constant power, while the stator current was not increased beyond rated vale during wide-speed range operation. Utilizing the d-axis current decreased the flux density, thereby reducing the core losses, and ultimately resulting in high efficiency. However, in the existing topology, the stator current was increased to increase the torque for maintaining constant power during entire wide-speed range operation. This is because the torque was very low in differential mode. The core losses remained high, furthermore, increase in stator current resulted in high copper losses, and ultimately resulting in low efficiency compared to the proposed topology.

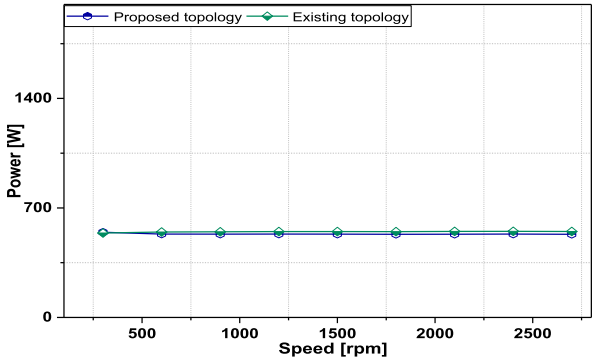

FIGURE 13. Comparison of power speed curves in proposed and existing topology.

Fig. 13 compares the power-speed curves of the proposed and existing topology. It can be observed that the power-speed curves of both topologies are almost the same. Furthermore, machine power remains approximately constant, during the entire wide-speed operation. However, to maintain constant power, the torque of the machine has been decreased as speed increased. The overall performance comparison of the PMVM for both modes in the proposed and existing topology is presented in Table 3.

V. CONCLUSION

This paper proposes two modes of operation for a PMVM to improve efficiency and wide-speed range operation, using a single inverter. In mode-1, a high torque was achieved with the stator winding connected in a wye configuration. In mode-2, a wide-speed range was achieved with the stator winding connected in a wye-delta configuration. The winding switching, for changing modes, was fabricated by using six additional bi-directional low-cost thyristor switches. The results were compared to the existing dual-inverter PMVM topology. The proposed PMVM showed less losses, and consequently improved efficiency, compared to the existing topology. Furthermore, the two inverters used in the existing topology were replaced by a single inverter in the proposed topology, which consequently reduced the cost. The maximum speed achieved by the proposed topology was less than that of the existing topology; however, due to its higher efficiency and low cost the proposed PMVM could be a better candidate for small EVs; such as golf carts. The

experiment of the proposed idea will be provided in future research paper.

REFERENCES

[1] B. Kim and T. A. Lipo, "Operation and design principles of a PM Vernier motor," *IEEE Trans. Ind. Appl.*, vol. 50, no. 6, pp. 3656–3663, Nov./Dec. 2014, doi: 10.1109/TIA.2014.2313693.

[2] F. Zhao, T. A. Lipo, and B.-I. Kwon, "Dual-stator interior permanent magnet Vernier machine having torque density and power factor improvement," *Electr. Power Compon. Syst.*, vol. 42, no. 15, pp. 1717–1726, Nov. 2014.

[3] X. Sun, B. Su, S. Wang, Z. Yang, G. Lei, J. Zhu, and Y. Guo, "Performance analysis of suspension force and torque in an IBPMSM with V-shaped PMs for flywheel batteries," *IEEE Trans. Magn.*, vol. 54, no. 11, Nov. 2018, Art. no. 8105504, doi: 10.1109/TMAG.2018.2827103.

[4] Z. Shi, X. Sun, Y. Cai, Z. Yang, G. Lei, Y. Guo, and J. Zhu, "Torque analysis and dynamic performance improvement of a PMSM for EVs by skew angle optimization," *IEEE Trans. Appl. Supercond.*, vol. 29, no. 2, Mar. 2019, Art. no. 0600305, doi: 10.1109/TASC.2018.2882419.

[5] X. Sun, Z. Jin, S. Wang, Z. Yang, K. Li, Y. Fan, and L. Chen, "Performance improvement of torque and suspension force for a novel five-phase BFSPM machine for flywheel energy storage systems," *IEEE Trans. Appl. Supercond.*, vol. 29, no. 2, Mar. 2019, Art. no. 0601505, doi: 10.1109/TASC.2019.2893295.

[6] J. Li, K. T. Chau, J. Z. Jiang, C. Liu, and W. Li, "A new efficient permanent-magnet Vernier machine for wind power generation," *IEEE Trans. Magn.*, vol. 46, no. 6, pp. 1475–1478, Jun. 2010.

[7] J. Yang, G. Liu, W. Zhao, Q. Chen, Y. Jiang, L. Sun, and X. Zhu, "Quantitative comparison for fractional-slot concentrated-winding configurations of permanent-magnet Vernier machines," *IEEE Trans. Magn.*, vol. 49, no. 7, pp. 3826–3829, Jul. 2013.

[8] T. Zou, D. Li, R. Qu, D. Jiang, and J. Li, "Advanced high torque density PM Vernier machine with multiple working harmonics," *IEEE Trans. Ind. Appl.*, vol. 53, no. 6, pp. 5295–5304, Nov. 2017.

[9] T. Zou, D. Li, C. Chen, R. Qu, and D. Jiang, "A multiple working harmonic PM Vernier machine with enhanced flux-modulation effect," *IEEE Trans. Magn.*, vol. 54, no. 11, Nov. 2018, Art. no. 8109605.

[10] N. Baloch, B.-I. Kwon, and Y. Gao, "Low-cost high-torque-density dual-stator consequent-pole permanent magnet Vernier machine," *IEEE Trans. Magn.*, vol. 54, no. 11, Nov. 2018, Art no. 8206105, doi: 10.1109/TMAG.2018.2849082.

[11] X. Ren, D. Li, R. Qu, Z. Yu, and Y. Gao, "Investigation of spoke array permanent magnet Vernier machine with alternate flux bridges," *IEEE Trans. Energy Convers.*, vol. 33, no. 4, pp. 2112–2121, Dec. 2018.

[12] Y. Gao, D. Li, R. Qu, H. Fang, H. Ding, and L. Jing, "Analysis of a novel consequent-pole flux switching permanent magnet machine with flux bridges in stator core," *IEEE Trans. Energy Convers.*, vol. 33, no. 4, pp. 2153–2162, Dec. 2018, doi: 10.1109/TEC.2018.2839727.

[13] Z. Liang, Y. Gao, D. Li, and R. Qu, "Design of a novel dual flux modulation machine with consequent-pole spoke-array permanent magnets in both stator and rotor," *CES Trans. Electr. Mach. Syst.*, vol. 2, no. 1, pp. 73–81, Mar. 2018, doi: 10.23919/TEMS.2018.8326453.

[14] F. Zhao, T. A. Lipo, and B.-I. Kwon, "A novel dual-stator axial-flux spoke-type permanent magnet Vernier machine for direct-drive applications," *IEEE Trans. Magn.*, vol. 50, no. 11, Nov. 2014, Art. no. 8104304, doi: 10.1109/TMAG.2014.2329861.

[15] B. Kim and T. A. Lipo, "Analysis of a PM Vernier motor with spoke structure," *IEEE Trans. Ind. Appl.*, vol. 52, no. 1, pp. 217–225, Jan./Feb 2016, doi: 10.1109/TIA.2015.2477798.

[16] D. Li, R. Qu, and T. A. Lipo, "High-power-factor Vernier permanent-magnet machines," *IEEE Trans. Ind. Appl.*, vol. 50, no. 6, pp. 3664–3674, Nov./Dec. 2014.

[17] S. Atiq, T. A. Lipo, and B.-I. Kwon, "Wide speed range operation of non-salient PM machines," *IEEE Trans. Energy Convers.*, vol. 31, no. 3, pp. 1179–1191, Sep. 2016, doi: 10.1109/TEC.2016.2547421.

[18] A. Arif, N. Baloch, and B. I. Kwon, "Wide speed range operation of permanent magnet Vernier machines," *Electron. Lett.*, vol. 54, no. 18, pp. 1070–1072, Sep. 2018, doi: 10.1049/el.2018.5008.

[19] A. Arif, N. Baloch, and B.-I. Kwon, "Winding switching and turn switching in permanent magnet Vernier machines for wide speed range operation and high efficiency," *IEEE Access*, vol. 7, pp. 55344–55357, 2019, doi: 10.1109/ACCESS.2019.2912181.

[20] H. Huang and L. Chang, "Electrical two-speed propulsion by motor winding switching and its control strategies for electric vehicles," *IEEE Trans. Veh. Technol.*, vol. 48, no. 2, pp. 607–618, Mar. 1999.

[21] M.-S. Lim and J.-P. Hong, "Design of high efficiency wound field synchronous machine with winding connection change method," *IEEE Trans. Energy Convers.*, vol. 33, no. 4, pp. 1978–1987, Dec. 2018.

[22] M. Ayub, S. Atiq, G. J. Sirewal, and B.-I. Kwon, "Fault-tolerant operation of wound field synchronous machine using coil switching," *IEEE Access*, vol. 7, pp. 67130–67138, 2019.

[23] T. Gerrits, C. G. E. Wijnands, J. J. H. Paulides, and J. L. Duarte, "Fault tolerant operation of a fully electric gearbox equivalent," *IEEE Trans. Ind. Appl.*, vol. 48, no. 6, pp. 1855–1865, Nov. 2012.

[24] M.-S. Wang, N.-C. Hsu, C.-Y. Chiang, S.-H. Wang, and T.-C. Shau, "A novel changeover technique for variable-winding brushless DC motor drives," in *Proc. SICE Annu. Conf.*, Taipei, Taiwan, 2010, pp. 2650–2653.

[25] T. Kume and T. Sawa, "A static winding changeover technique," Japanese Patent 799 959, Oct. 25, 1995.

[26] M. M. Swamy, T. Kume, A. Maemura, and S. Morimoto, "Extended high-speed operation via electronic winding-change method for AC motors," *IEEE Trans. Ind. Appl.*, vol. 42, no. 3, pp. 742–752, May/Jun. 2006.

[27] H. Vansompel, P. Sergeant, L. Dupre, and A. Bossche, "A combined wye-delta connection to increase the performance of axial-flux PM machines with concentrated windings," *IEEE Trans. Energy Convers.*, vol. 27, no. 2, pp. 403–410, Jun. 2012.

[28] Y. Lei, Z. Zhao, S. Wang, D. G. Dorrell, and W. Xu, "Design and analysis of star–delta hybrid windings for high-voltage induction motors," *IEEE Trans. Ind. Electron.*, vol. 58, no. 9, pp. 3758–3767, Sep. 2011.

[29] M. N. Ibrahim, P. Sergeant, and E. E. M. Rashad, "Combined star–delta windings to improve synchronous reluctance motor performance," *IEEE Trans. Energy Convers.*, vol. 31, no. 4, pp. 1479–1487, Dec. 2016, doi: 10.1109/TEC.2016.2576641.

[30] M. N. F. Ibrahim, E. Rashad, and P. Sergeant, "Performance comparison of conventional synchronous reluctance machines and PM-assisted types with combined star–delta winding," *Energies*, vol. 10, no. 10, p. 1500, 2017.

[31] H. Wang, S. Fang, H. Yang, H. Lin, D. Wang, Y. Li, and C. Jiu, "A novel consequent-pole hybrid excited Vernier machine," *IEEE Trans. Magn.*, vol. 53, no. 11, Nov. 2017, Art. no. 8112304, doi: 10.1109/TMAG.2017.2695494.

[32] G. Bertotti, *Hysteresis in Magnetism: For Physicists, Materials Scientists, and Engineers*. Waltham, MA, USA: Academic, 1998.

ARSALAN ARIF was born in 1984. He received the B.S. degree in electrical engineering from the University of Engineering and Technology (UET), Peshawar, Pakistan, in 2006, and the M.S. degree in electronics system engineering and the Ph.D. degree in electrical and electronic engineering from Hanyang University, Ansan, South Korea, in 2010 and February 2020, respectively. From 2010 to 2013, he was a Lecturer with the Sarhad University of Science and Information Technology (SUIT), Pakistan. He is currently a Postdoctoral Fellow with the Energy Conversion Laboratory, Hanyang University. His research interests include control and design of electrical machines.

NOMAN BALOCH was born in Pakistan. He received the B.S. degree in electronics engineering from the Balochistan University of Information Technology, Engineering and Management Sciences (BUITEMS), Quetta, Pakistan, in 2010, and the Ph.D. degree in electrical and electronic engineering from Hanyang University, South Korea, in February 2020.

From 2010 to 2015, he was a Deputy Assistant Director with the National Database and Registration Authority (NADRA), Pakistan. He is currently a Postdoctoral Fellow with the Energy Conversion Laboratory, Hanyang University, South Korea. His research interests include design and control of electrical machines.

MUHAMMAD AYUB was born in Quetta, Pakistan. He received the B.S. degree from the Balochistan University of Information Technology, Engineering and Management Sciences (BUITEMS), Quetta, in 2008, and the Ph.D. degree from the Department of Electrical and Electronic Engineering, Hanyang University, Ansan, South Korea. He was a Lecturer with BUITEMS. His research interests include electric machine design, optimization, and control.

BYUNG-IL KWON (Senior Member, IEEE) was born in 1956. He received the B.S. and M.S. degrees in electrical engineering from Hanyang University, Ansan, South Korea, in 1981 and 1983, respectively, and the Ph.D. degree in electrical engineering, machine analysis from The University of Tokyo, Tokyo, Japan, in 1989. From 1989 to 2000, he was a Visiting Researcher with the Faculty of Science and Engineering Laboratory, University of Waseda, Tokyo. In 1990, he was a Researcher with the Toshiba System Laboratory, Yokohama, Japan. In 1991, he was a Senior Researcher with the Institute of Machinery and Materials Magnetic Train Business, Daejeon, South Korea. From 2001 to 2008, he was a Visiting Professor with the University of Wisconsin–Madison, Madison, WI, USA. He is currently a Professor with Hanyang University. His research interests include design and control of electric machines.